J. Fluid Mech. (1979), *vol.* 95, *part* 4, *pp.* 655–679
Printed in Great Britain

The representation of the viscous wall region by a regular eddy pattern

By DIMITRIOS T. HATZIAVRAMIDIS AND THOMAS J. HANRATTY
Department of Chemical Engineering, University of Illinois, Urbana

(Received 9 March 1978 and in revised form 27 March 1979)

A model for the kinematics of a turbulent flow close to a solid boundary is explored. The field is assumed to be homogeneous in the direction of mean flow. The equations of motion are solved numerically for a flow which is periodic in time and in a direction transverse to the direction of mean flow. The period is taken to be the time interval between 'bursts' and the wavelength, the spacing of the streaky structure close to the wall observed by a number of investigators. Good agreement is obtained between the calculated flow field and experimental results, especially for $y^+ < 15$. This agreement suggests that the flow oriented eddies in the viscous wall region can be represented by a model which views the flow in this region to be coherent and to be associated with spanwise flow deviations in a well-mixed outer region. The model allows for the periodic movement of low momentum fluid from the wall, which, because of the assumption of a well mixed outer region, gives rise to a shear layer. This seems to correspond to the observed 'bursting' phenomenon. The calculations confirm the suggestion by Fortuna and Hanratty (Fortuna 1970; Hanratty, Chorn & Hatziavramidis 1977) that the secondary flow in the viscous wall region generated by these spanwise flow deviations gives rise to the development of large velocity fluctuations in the direction of mean flow and accounts for the experimentally observed maximum in the velocity fluctuations close to the wall. Also, the comparison of calculations with measurements of the average velocity and with an experimental quadrant analysis of the Reynolds stress suggests that the secondary flow is making a major contribution to the Reynolds stress.

1. Introduction

The viscous wall region of a turbulent flow is the region close to a wall where viscosity makes a significant direct contribution to the transfer of momentum. It occupies the space between $y^+ = 0$ and $y^+ = c.\ 30$, where y^+ is the distance from the wall made dimensionless using the wall parameters, ν and $u^* = (\tau_w/\rho)^{\frac{1}{2}}$. In recent years considerable attention has been given to the discovery that turbulent flow in the viscous wall region is coherent and that repetitive processes can be identified that seem to play an important role in the production of turbulence.

This interest was initiated by Beatty, Ferrell and Richardson (Corrsin 1956) who pumped dye solution through a pipe and, after flushing with water, observed the formation of the residual dye into streamwise filaments at the wall. The existence of this streaky structure was confirmed by Hama (Corrsin 1956), who injected dye

0022–1120/79/4335–7750 $02.00

through a wall slot. However, Kline and his co-workers (Kline & Runstadler 1959; Kim, Kline & Reynolds 1971; Kline *et al.* 1967) through the extensive utilization of these dye techniques, as well as hydrogen bubble techniques, properly interpreted these results. They showed that the wall dye streaks are regions of low axial velocities and that after lifting from the wall, the streaks undergo a strong interaction, called a 'burst', with the turbulent fluid outside the viscous wall region. A number of laboratories have confirmed these results and have added additional qualitative and quantitative information about the kinematics of the viscous wall layer. The two chief structural parameters which have resulted from these studies are the definition of the spacing between streaks, λ, and the period between bursts, T_B.

The two dominant theoretical notions that have been used to account for the kinematic behaviour of the viscous wall region have been that the region is driven by the flow outside or that the events are due to a hydrodynamic instability. The latter explanation has been particularly emphasized in recent works of Mollo-Christensen (1971), Landahl (1972), Blackwelder & Kaplan (1972) because of the 'apparently' spectacular events associated with 'bursting'.

The present paper uses the notion of a driven flow in that it associates flow patterns close to the wall with velocity fluctuations in a well mixed outer region. It shows that a regular eddy model with length and time scales given by presently available structural information is consistent with visual observations and quantitative measurements of turbulence in the wall region. However, since the model does not specify the origin of the flow fluctuations in the outer flow it does not really answer the question of whether the flow in the viscous wall region is 'driving' the outer flow or just responding passively.

The first treatment of the fluctuating flow in the viscous wall region as a response to the outside flow was by Taylor (1932). In order to explain measurements of the spatial variation of turbulent velocity fluctuations close to a wall by Fage & Townsend (1932), Taylor assumed that the fluctuating flow in the immediate vicinity of the wall is a response to pressure fluctuations imposed by the outer flow. He used a truncated form of the linearized momentum equations to relate the velocity field to the pressure field. This type of linear analysis was later carried out by Sternberg (1962, 1965), Schubert & Corcos (1967) and Gurkham & Kader (1970). More recently Hatziavramidis (1978) has shown that linear theory can be used only to describe the high frequency fluctuations and that nonlinear effects will have to be taken into account to describe the energy containing fluctuations.

The realization that the linearized momentum equations do not properly take into account the Reynolds stresses prompted Fortuna and Hanratty (Fortuna 1970; Hanratty *et al.* 1977) to take a different approach in describing the interaction between the viscous wall region and the outer flow. They assumed that flow just outside the viscous wall region is primarily in the direction of mean flow. Spanwise deviations in these flow lines can be associated with small velocity fluctuations in the transverse direction which are dampened close to the wall by viscous effects. From a consideration of the law of conservation of mass Fortuna and Hanratty assumed that the viscous dampening of these flow deviations gives rise to secondary flows of the type shown in figure 1. These secondary flows bring excess x momentum to the wall, exchange momentum with the wall, and then carry momentum deficient fluid away from the wall. Consequently, as indicated in figure 1, the two components of the

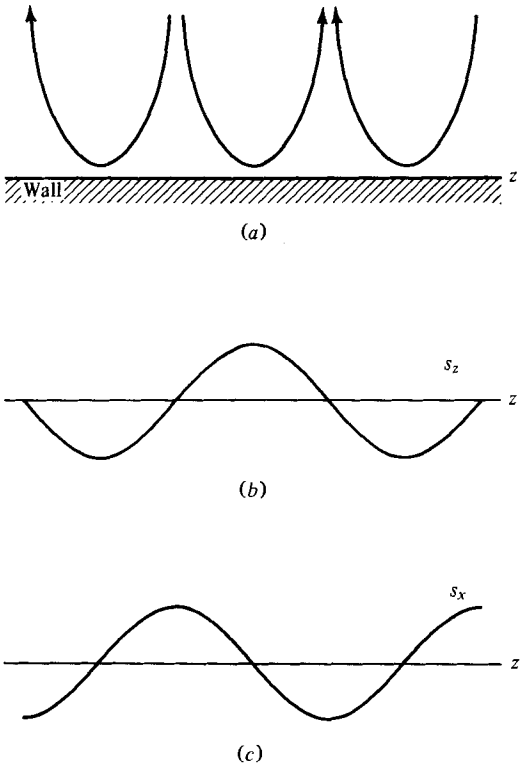

FIGURE 1. Idealized eddy pattern at the wall.

velocity gradient at the wall, s_x and s_z, would have spanwise variations which are out of phase by approximately $\frac{1}{4}\lambda$. Fortuna and Hanratty assumed that the transverse velocity component associated with the secondary flow is homogeneous in the direction of mean flow, and varies harmonically in the transverse direction and randomly in time

$$w = \hat{w}(t) f(y) \sin(2\pi z/\lambda). \tag{1}$$

The parameter λ was selected to agree with the observed streak spacing, $\hat{w}(t)$ was assumed to be given by a Gaussian distribution and $\overline{\hat{w}^2}$ was selected so as to be consistent with Laufer's measurements of mean-squared values of the turbulent fluctuating velocity. For simplicity $f(y)$ was set equal to y. The velocity component normal to the wall was calculated from the law of conservation of mass using the assumption that the flow is homogeneous in the x direction. The velocity in the x direction $U(y, z, t)$ was calculated from the x momentum equation using the boundary condition that $U = U_L$ for large y. The parameter U_L was selected so that the calculated average velocity profile agreed with Newton's law of viscosity at small y. In order to solve the momentum equation Fortuna and Hanratty argued that the energy containing eddies close to the wall were of low enough frequency that a pseudosteady-state assumption could be made whereby the transient term $\rho\,\partial U/\partial t$ could be neglected.

The analysis of Fortuna and Hanratty was largely motivated by the results of measurements of the two components of the fluctuating velocity gradient, s_x and s_z,

at multiple locations on a wall using electrochemical probes which are the mass transfer analogue of the hot film probe. The measurements of the spatial correlation coefficients of s_x and s_z by Mitchell & Hanratty (1966), Fortuna, Gilead & Hanratty (1972) and Chorn (Hanratty *et al.* 1977) clearly show that scales in the x direction are about 40 times the scales in the z direction and therefore support the assumption of homogeneity in mean flow direction. Simultaneous measurements of s_z at a number of locations by Eckelman (1971) gave no evidence that close to the wall outflows are much more intense than inflows. More recent measurements by Lee, Eckelman & Hanratty (1974) show the relative phases of the functions describing the spatial variation of s_x and s_z are what would be expected from such a model. Even though the calculations by Fortuna and Hanratty gave good agreement with measured time averaged velocities and with the observed relation between polymer drag-reduction and λ (Hanratty *et al.* 1977), the model has a number of difficulties. The chief of these is the assumption that the energy containing eddies can be represented by a pseudo-steady state assumption.

In this paper the formulation of Fortuna and Hanratty is extended by including transient terms and by solving the nonlinear momentum equations for the secondary flow rather than making *ad hoc* assumptions regarding the spatial variation of w.

The nonlinear model explored in the work assumes that a coherent motion exists for $0 < y^+ < 30$–50 and that the region beyond $y^+ > 30$–50 is well mixed. The transverse flow at the edge of the viscous wall layer is assumed to be given by the regular function

$$w = w_L \sin\frac{2\pi z}{\lambda} \cos \omega t. \tag{2}$$

Here λ and ω are assumed to be approximately equal to the spacing of the dye streaks and the frequency of bursting, and w_L is a constant. The secondary flow is calculated by seeking a periodic solution of the non-steady Navier–Stokes equation, simplified by assuming the flow is homogeneous in the direction of mean flow. Because of this latter assumption, the y and z momentum equations are decoupled from the x momentum equations. After the secondary flow is calculated, the unsteady x momentum equation is solved assuming that the velocity in the mixed region is given by measurements of the average velocity.

The assumption of coherency is employed in these calculations by allowing the calculated flow field for $y^+ < y_0^+$ to be completely deterministic. In addition, no attempt is made to account for the effect of small scale disturbances by including turbulent stresses in the equations defining the secondary flow.

The approximation of a well mixed flow for $y^+ > y_0^+$ is motivated by experimental measurements of the velocity field. These show that the average velocity and the mean squared values of the three components of the fluctuating velocity vary rather slowly with distance from the wall for $y^+ > 30$. However, because of the presence of the wall, viscous dampening occurs and there is a very rapid variation of these quantities for $y^+ < 30$. The model attempts to characterize this viscous interaction of the turbulent flow with the wall. Measurements of the transverse component of the fluctuating velocity gradient at the wall suggest that very close to the wall the dominant period characterizing the variation of the transverse component of the fluctuating velocity, w, is approximately equal to the spacing of the streaky structure (Lee *et al.* 1974). Furthermore, measurements at $y^+ = 8$ of the instantaneous variation

of the lateral component of the turbulent velocity fluctuations, w, in the lateral direction (see figure 3–30, Schraub & Kline 1965) show that the magnitude of $\partial w/\partial z$ does not depend on its sign. The simplest function characterizing the spatial variation of w at the edge of the viscous wall region which is consistent with the above observations and the observations that turbulence properties at the wall are approximately homogeneous in the direction of flow is equation (2).

Observations of the instantaneous values of s_z at a number of locations on the wall reveal the existence of spatial variations of s_z of a smaller scale than λ. The model assumes these are contributing a small part to the total energy of the w velocity fluctuations so that w_L may be approximated from measurements of the intensity of turbulence at $y^+ \cong 30$.

However, these small-scale fluctuations can be characterized by rather large values of $\partial w/\partial z$. Since, from the continuity equation the velocity component normal to the wall is given by

$$v = \int_0^y -\frac{\partial w}{\partial z}\, dy,$$

it is seen that small scale variations in w could be making large contributions to the normal velocity component. Consequently, it is envisioned that the v velocities associated with the eddies modelled in this paper could be much smaller than would be indicated by turbulence measurements very close to a wall.

2. Statement of the model

The average flow is assumed parallel to the x direction. By using the assumption of homogeneity in the x direction the velocity field is given by the equations

$$\frac{\partial w}{\partial t} + w\frac{\partial w}{\partial z} + v\frac{\partial w}{\partial y} = -\frac{1}{\rho}\frac{\partial P}{\partial z} + \nu\left(\frac{\partial^2 w}{\partial z^2} + \frac{\partial^2 w}{\partial y^2}\right), \tag{3}$$

$$\frac{\partial v}{\partial t} + w\frac{\partial v}{\partial z} + v\frac{\partial v}{\partial y} = -\frac{1}{\rho}\frac{\partial P}{\partial y} + \nu\left(\frac{\partial^2 v}{\partial z^2} + \frac{\partial^2 v}{\partial y^2}\right), \tag{4}$$

$$\frac{\partial U}{\partial t} + w\frac{\partial U}{\partial z} + v\frac{\partial U}{\partial y} = \nu\left(\frac{\partial^2 U}{\partial z^2} + \frac{\partial^2 U}{\partial y^2}\right), \tag{5}$$

$$\frac{\partial w}{\partial z} + \frac{\partial v}{\partial y} = 0. \tag{6}$$

These are to be solved subject to boundary conditions

$$z = 0, \quad \tfrac{1}{2}\lambda, \quad w = 0, \quad \frac{\partial v}{\partial z} = 0, \quad \frac{\partial U}{\partial z} = 0, \tag{7}$$

$$y = 0, \quad w = v = U = 0, \tag{8}$$

$$y = y_0, \quad w = w_L \sin\frac{2\pi z}{\lambda}\cos\omega t, \tag{9}$$

v in accordance with (6),

$$U = \bar{U} + u \simeq U_L,$$

where U_L is the measured time average velocity at y_0. For this purpose we used the average velocity measurements given by Laufer (1954). For initial conditions we took w, v from the inviscid irrotational solution and $U = \bar{U}(y)$.

Equations (3), (4) and (6) can be reformulated in terms of the vorticity ζ and the *stream function* Ψ, *defined as*

$$w = -\frac{\partial \Psi}{\partial y}, \quad v = \frac{\partial \Psi}{\partial z}, \quad \zeta = \frac{\partial w}{\partial y} - \frac{\partial v}{\partial z}. \tag{10}$$

The new variables ζ and Ψ are related through the equation

$$\frac{\partial^2 \Psi}{\partial z^2} + \frac{\partial^2 \Psi}{\partial y^2} = -\zeta. \tag{11}$$

After eliminating the pressures between (3) and (4)

$$\frac{\partial \zeta}{\partial t} - \frac{\partial \Psi}{\partial y}\frac{\partial \zeta}{\partial z} + \frac{\partial \Psi}{\partial z}\frac{\partial \zeta}{\partial y} = \nu\left(\frac{\partial^2 \zeta}{\partial z^2} + \frac{\partial_2 \zeta}{\partial y^2}\right). \tag{12}$$

The boundary conditions for (11) and (12) are

$$z = 0, \tfrac{1}{2}\lambda, \quad \Psi = 0, \quad \zeta = 0,$$

$$y = 0, \quad \Psi = 0, \quad \frac{\partial \Psi}{\partial y} = 0, \tag{13}$$

$$y = y_0, \quad \frac{\partial \Psi}{\partial y} = -w_L \sin\frac{2\pi z}{\lambda}, \quad \cos\omega t \frac{\partial^2 \Psi}{\partial y^2} = 0, \tag{14}$$

$$t = 0, \quad \Psi = -\frac{w_L \lambda}{2\pi}\sin\frac{2\pi z}{\lambda}\frac{\sinh(2\pi y/\lambda)}{\cosh(2\pi y_0/\lambda)}, \quad \zeta = 0. \tag{15}$$

Finite difference methods were used to find solutions of (11), (12) and (5). The field was divided into 32 increments in the y direction and 26 increments in the z direction. The time step was selected so as to satisfy the Neumann condition

$$\frac{\Delta t}{\lambda w_L}\left(\frac{1}{\Delta z^2} + \frac{1}{\Delta y^2}\right) \leqslant \tfrac{1}{2}. \tag{16}$$

The vorticity equation (12) and the x momentum equation were solved using the alternating direction implicit method which was introduced by Peaceman & Rachford (1955). The stream function equation was solved using the successive over-relaxation method known as the 'extrapolated Liebmann method'. The proposal of Frankel (1950) was found to give a good estimate of the relaxation factor for the present calculations.

In the finite difference approximation of the vorticity equation, the calculation of vorticity values at time n from those at time $n-1$ in two steps yields two systems of equations which are respectively implicit in the z and y directions. These equations contain values of Ψ at the $n+\frac{1}{2}$ and $n+1$ time steps. Direct calculation of ζ^{n+1} and Ψ^{n+1} would require the implicit coupled solution of the finite difference approximation of the ζ and Ψ equations. In order to avoid this we have used the iterative procedure suggested by Pearson (1965) and Aziz & Hellums (1967). The boundary conditions for ζ at $y = y_0$ and $y = 0$ were approximated by

$$\zeta_{i,1} = \frac{8\Psi_{i,2} - \Psi_{i,3}}{2\Delta y^2}, \tag{17}$$

$$\zeta_{i,J} = \frac{\Psi_{i+1,J} + \Psi_{i-1,J} - 2\Psi_{i,J}}{\Delta z^2}, \tag{18}$$

where $(i, 1)$ denotes grid points at the wall and (i, J) denotes grid points at y_0.

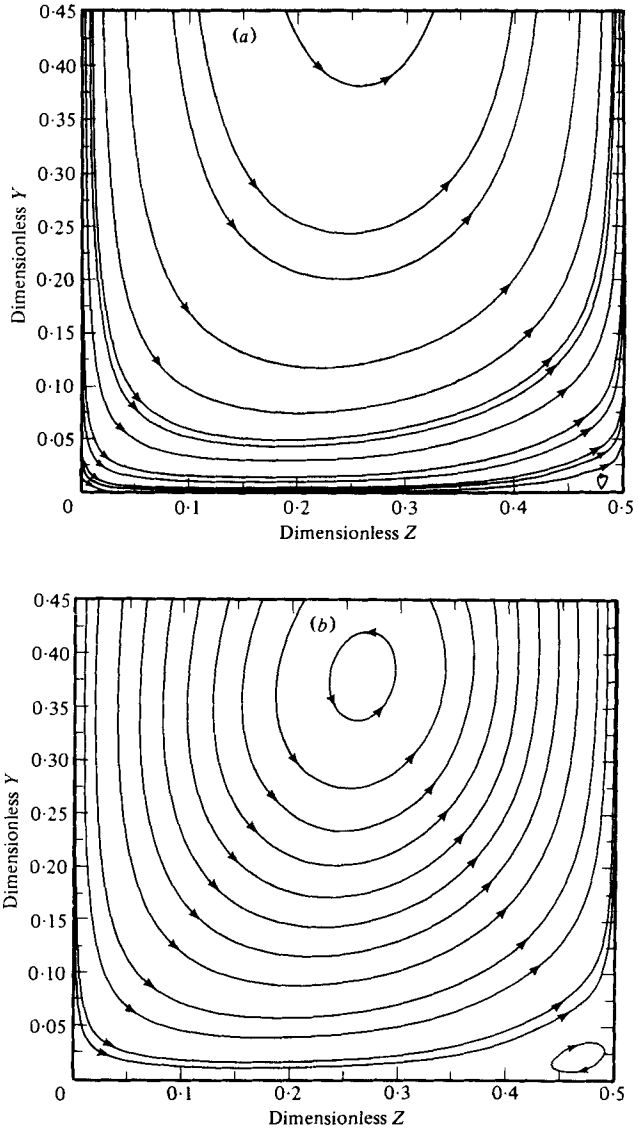

FIGURE 2 (*a*, *b*). For legend see page 665.

Details regarding the numerical procedures and the stability of the calculations can be found in a thesis by one of the authors (Hatziavramidis 1978).

Calculated values of ζ, Ψ, and U were found to vary periodically with time after 4–5 periods. The characteristics of this periodic solution are discussed in the remainder of this paper.

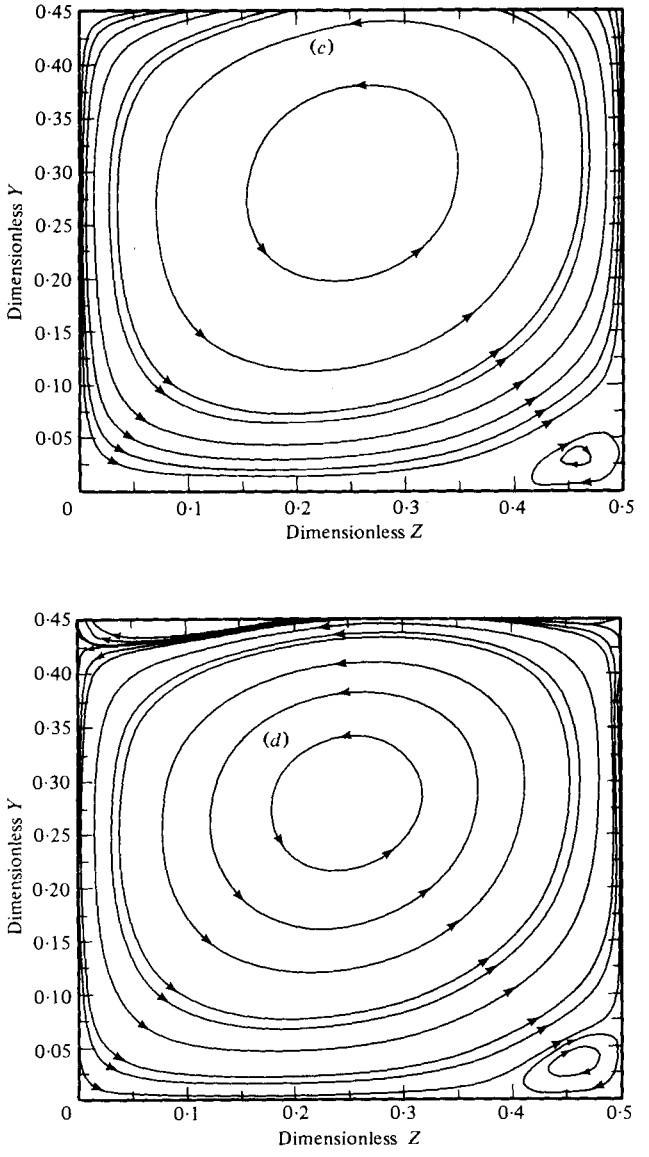

FIGURE 2(c, d). For legend see page 665.

3. Secondary flow patterns

Calculations of the stream function have been carried out by Hatziavramidis (1978) for the conditions $y_0^+ = 45$, $\lambda^+ = 100$, $T_B^+ = 100$ and $y_0^+ = 32$, $\lambda^+ = 100$, $T_B^+ = 100$, where T_B is the period defined as $2\pi/f$ and superscript $^+$ denotes quantities made dimensionless with friction velocity u^* and kinematic viscosity ν. The results for these two cases are similar so only the $y_0^+ = 45$ secondary flow patterns are presented here.

Figure 2 shows the evolution of secondary flow throughout a period of time approximately equal to one half the experimentally determined bursting period. The

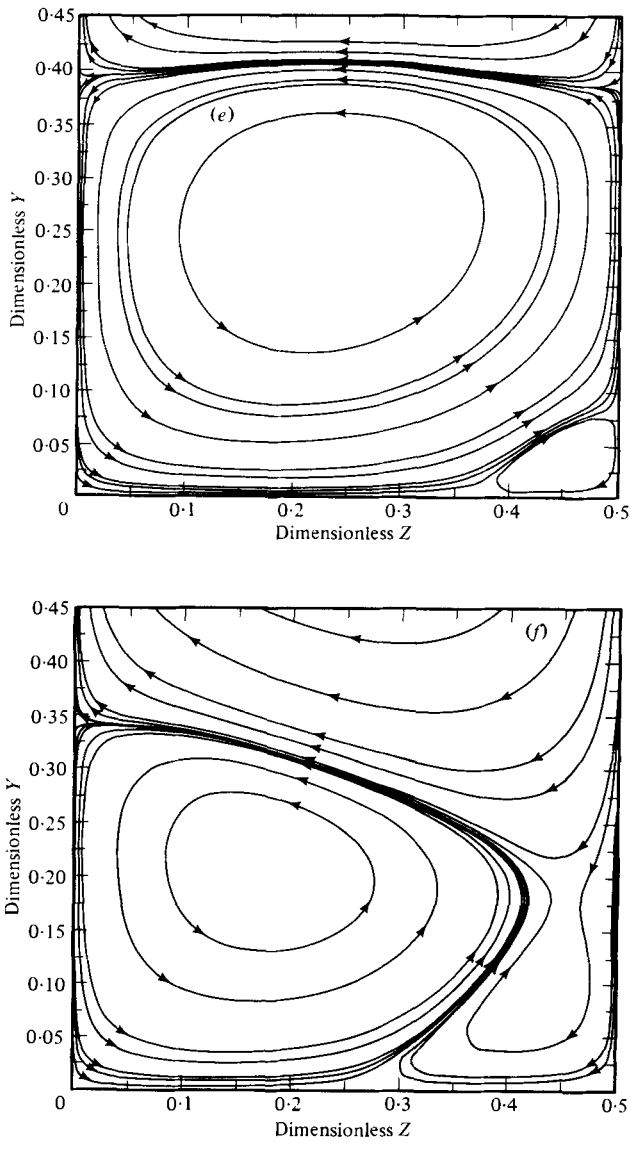

FIGURE 2 (*e*, *f*). For legend see page 665.

streamlines showing the main trends of the secondary flow are plotted at times selected to illustrate the variety of flow patterns. Consequently they are not equally spaced in time.

At $t = 0$ the flow pattern shows a strong inflow at $z = 0$ and a strong outflow at $z = \frac{1}{2}\lambda$. At $t = 0{\cdot}21T_B$ a small separation bubble appears close to the wall in the region of the outgoing flow. Because of the imposed outer boundary condition the w velocity reverses direction at $t = 0{\cdot}25T_B$. At $t = 0{\cdot}26T_B$ a streamwise vortex larger than the separation bubble appears close to the upper boundary. In subsequent times the streamwise vortex and the separation bubble increase in size, until at $t = 0{\cdot}31T_B$ the vortex occupies the whole region of coherency. At $t = 0{\cdot}31T_B$ the vortex reverses direction at the upper boundary. In subsequent times the separation bubble and the

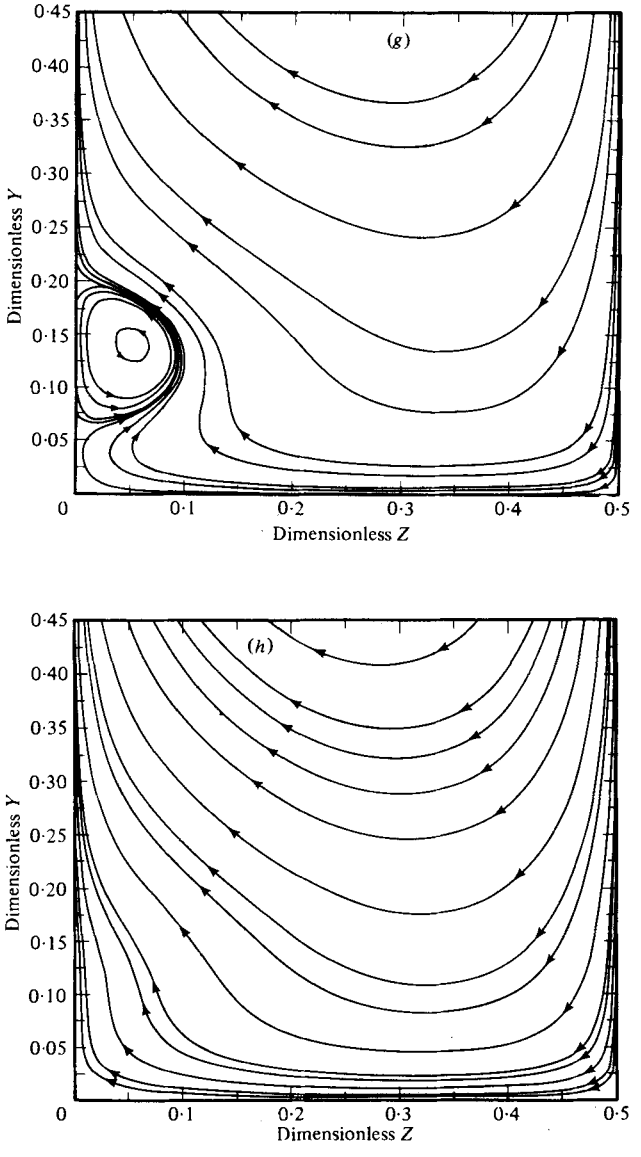

FIGURE 2(*g*, *h*). For legend see page 665.

streamwise vortex shrink in size until they eventually disappear. During this period the outflow at $z = 0$ and the inflow at $z = \frac{1}{2}\lambda$ become stronger and the secondary flow pattern shows phase changes as well as shear layers. See, for example, $t = 0{\cdot}39T_B$ and $t = 0{\cdot}44T_B$ in figure 2. At $t = 0{\cdot}50T_B$ the pattern is the same as for $t = 0$ except that the direction of flow is reversed. It is noted from the imposed boundary conditions that at $t = 0$ the transverse flow at y_0 has its maximum. This velocity decreases with increasing time until at $t = 0{\cdot}25T_B$ it changes direction. From $t = 0{\cdot}25T_B$ to $t = 0{\cdot}45T_B$ the flow field is in a transitional stage during which the whole flow field changes direction. The transition is characterized by the presence of vortical flows and of shear layers.

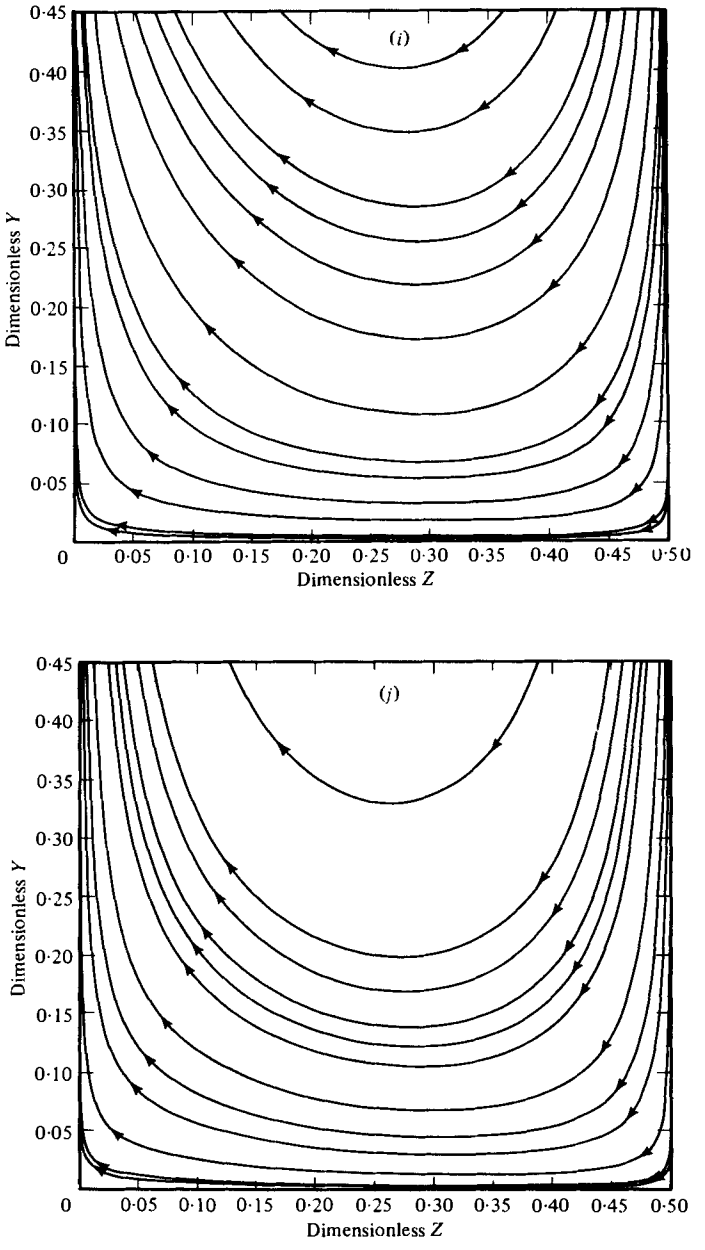

FIGURE 2. Calculated secondary flow pattern, $y_0^+ = 47$, $\lambda^+ = 100$ and $T_B^+ = 100$. (*a*) $t = 0{\cdot}21T_B$; (*b*) $t = 0{\cdot}26T_B$; (*c*) $t = 0{\cdot}31T_B$; (*d*) $t = 0{\cdot}32T_B$; (*e*) $t = 0{\cdot}34T_B$; (*f*) $t = 0{\cdot}39T_B$; (*g*) $t = 0{\cdot}44T_B$; (*h*) $t = 0{\cdot}45T_B$; (*i*) $t = 0{\cdot}49T_B$; (*j*) $t = 0{\cdot}59T_B$.

From $t = 0{\cdot}45T_B$ to $t = 0{\cdot}75T_B$ the w velocity component is negative throughout the field with the exception of the small separation bubble that appears at $t = 0{\cdot}71T_B$. The period $t = 0{\cdot}75 - 0{\cdot}95T_B$ is another transition period in which the w velocity changes direction throughout the field. Thus these transitional structures appear for about 40 percent of the time.

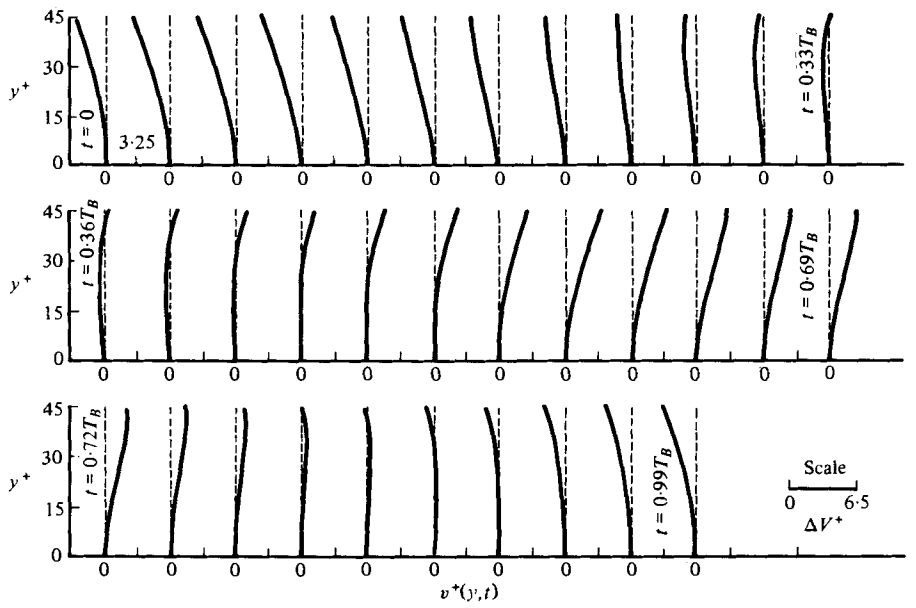

FIGURE 3. Calculated instantaneous normal velocity profiles, $y_0^+ = 45$, $\lambda^+ = 100$ and $T_B^+ = 100$, at $Z^+ = 0$ and for times $t = 0$ to $t = 0{\cdot}99T_B$.

These results appear consistent with visual studies of the wall region. For example, Brodkey and his co-workers (figure 4 in Brodkey *et al.* 1974) found that, on the average, ejections of low speed fluid occur 30 per cent of the time, inrushes of high-speed fluid occur 30 per cent of the time and interactions between ejections and inrushes occur 40 per cent of the time. The small separation bubbles appearing at $t = 0{\cdot}21T_B$ and the streamwise vortices in the final stages of their shrinkage also appear to exhibit many of the characteristics of the 'recirculation cells' described by Offen & Kline (1975).

The flow lines shown in figure 2 would suggest that dye injected through a wall slot would initially form a rising plume at $\frac{1}{2}\lambda$. At about $t = 0{\cdot}39T_B$ this plume would disappear at $\frac{1}{2}\lambda$ and would start to appear at $z = 0$ at about $t = 0{\cdot}44T_B$. However, before disappearing at $\frac{1}{2}\lambda$ it recedes toward the wall, perhaps giving the appearance of an oscillation, and has a lateral movement. This resembles in some ways the description of breakup given by Offen & Kline (see figure 2 of their paper, 1975).

The streamwise vortices observed over a part of the cycle are different from the counter-rotating eddies proposed by Townsend (1956) and Bakewell & Lumley (1967). The secondary flow velocity components are small when these vortices appear so they are not associated with intense outflows and inflows in the region of coherent motion. They exist only during transitional stages that separate periods during which the secondary velocities are large.

The calculations for $y_0^+ = 32$ have some slight differences from those just presented for $y_0^+ = 45$. The separation bubble appears earlier, $t = 0{\cdot}11T_B$ and $t = 0{\cdot}61T_B$ compared to $t = 0{\cdot}21T_B$ and $t = 0{\cdot}71T_B$, and grows to a larger size. The streamwise vortices are found to last for a shorter period, $t - 0{\cdot}26T_B - 0{\cdot}32T_B$ and $t = 0{\cdot}76T_B - 0{\cdot}82T_B$ compared to $t = 0{\cdot}26T_B - 0{\cdot}44T_B$ and $t = 0{\cdot}56T_B - 0{\cdot}94T_B$.

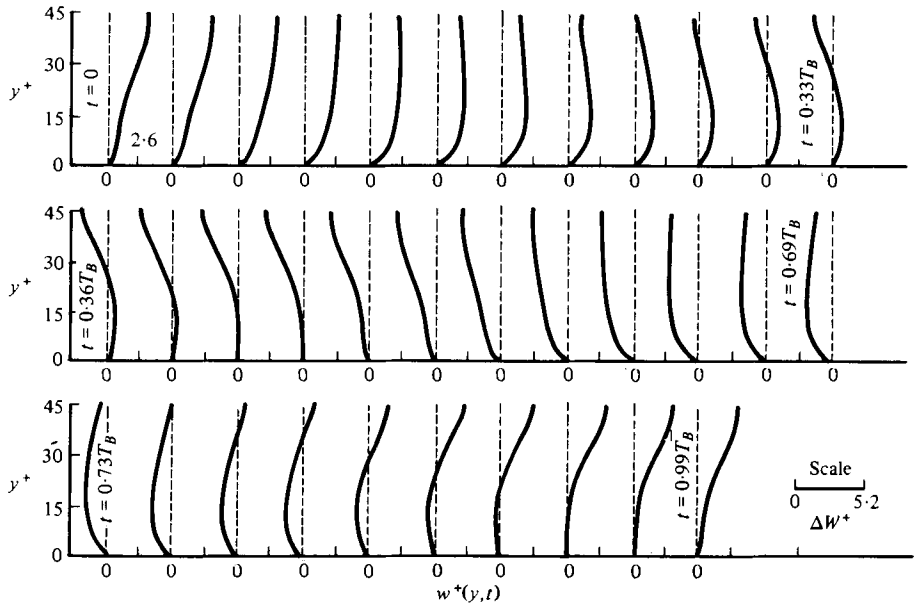

FIGURE 4. Calculated instantaneous velocity profiles, $y_0^+ = 45$, $\lambda^+ = 100$ and $T_B^+ = 100$, at $Z^+ = 24$ and for times $t = 0$ to $t = 0{\cdot}99T_B$.

4. Normal and transverse velocities

The magnitudes of the velocities associated with the secondary motion were studied by calculating $v(y,t)$ at $z = 0$ and $w(y,t)$ at $z = 0{\cdot}24\lambda$. Profiles of v and w at selected times are shown in figures 3 and 4. The horizontal dashed lines in these figures denote zero values of v or w. The velocity components are expressed in non-dimensionless form by normalizing with the friction velocity, $u^* = (\tau_w/\rho)^{\frac{1}{2}}$.

From figure 3 it is seen that the normal velocity component has a maximum amplitude of about $5u^*$ and that this occurs at $t = 0{\cdot}07T_B$ and $t = 0{\cdot}60T_B$. It is seen that strong inflows at $z = 0$ (large negative v velocities throughout the whole region $0 \leqslant y^+ \leqslant 45$) occur at times $t = 0$ to $0{\cdot}25T_B$ and $t = 0{\cdot}94T_B$. Strong outflows occur at $z = 0$ for $t = 0{\cdot}45T_B$ to $0{\cdot}75T_B$. Small values of v are observed for $t = 0{\cdot}26T_B$ to $0{\cdot}46T_B$ and $t = 0{\cdot}76T_B$ to $0{\cdot}93T_B$, when transitional patterns are shown to dominate the flow in figure 1. The v velocity reversed direction twice during a period, at $t = 0{\cdot}32T_B$ and $t = 0{\cdot}83T_B$. From figure 2 it is also seen that, on the average, close to the wall the v velocity component assumes larger magnitudes during inflows than during outflows. However, far from the wall, the v velocity has larger magnitudes for outflows, on the average, than it does for inflows.

In contrast to the v profiles, the w profiles shown in figure 4 are highly inflexional at certain times ($t = 0$ to $0{\cdot}06T_B$, $t = 0{\cdot}46T_B$ to $0{\cdot}54T_B$, and $t = 0{\cdot}96T_B$ to T_B) and show phase reversals at $t = 0{\cdot}26T_B$ to $0{\cdot}42T_B$ and $t = 0{\cdot}76T_B$ to $0{\cdot}92T_B$ when streamwise vortices dominate the flow. The w velocity components are also noted to assume their largest values during periods of strong inflows and outflows.

These calculations of the v and w velocity components show periods of high activity for the secondary flow (strong inflows and strong outflows) alternating with periods

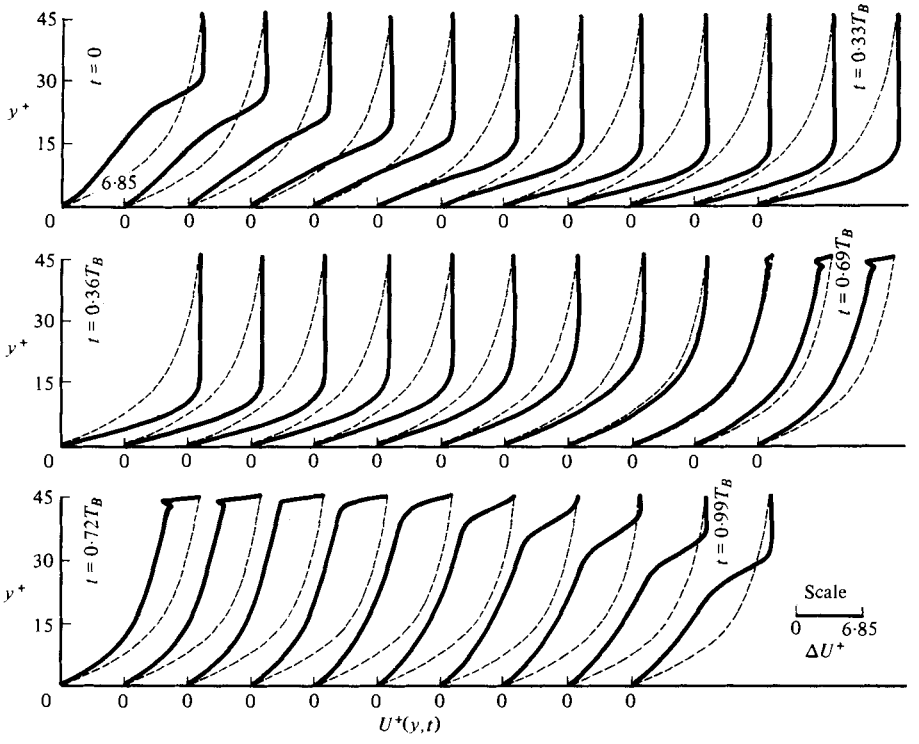

FIGURE 5. Calculated instantaneous axial velocity profile, $y_0^+ = 45$, $\lambda^+ = 100$ and $T_B^+ = 100$, at $Z^+ = 0$ and for times $t = 0$ to $t = 0{\cdot}99T_B$.

of low activity (transitional flows). Many of the features of these calculated velocity profiles appear to agree with experimental observation.

Corino & Brodkey (1969) and Grass (1971) have observed very large normal velocities during ejection (strong outflows) and sweep (strong inflow) stages. According to Corino & Brodkey the vertical velocity during the most active stages of coherent motions, ejections and sweeps, can be as large as 30 per cent of the axial velocity. Grass (1971) has also reported large transverse velocities as in a stagnation-type flow pattern associated with sweeps. Eckelmann (1974), Grass (1971) and Brodkey, Wallace & Eckelmann (1974) have observed that inflows are larger than outflows close to the wall and that outflows are stronger than inflows far from the wall.

5. Instantaneous axial velocity profiles

Calculated instantaneous axial velocity profiles at $z = 0$ and at $z = 0{\cdot}22\lambda$ are shown in figures 5 and 6. In these figures the time averaged velocity profiles are indicated by dashed lines.

The instantaneous axial profiles at $z = 0$ show positive deviations from the mean velocity profile far from the wall and negative deviations close to the wall at the beginning of the period ($t = 0$ to $t = 0{\cdot}13T_B$). Over the time $t = 0$ to $t = 0{\cdot}34T_B$ increases in the axial velocities are noted. This acceleration is stronger far from the wall. It is noted that this acceleration occurs at the same time that strong inflows occur at $z = 0$, so that it is associated with the convection of momentum from the outer flow

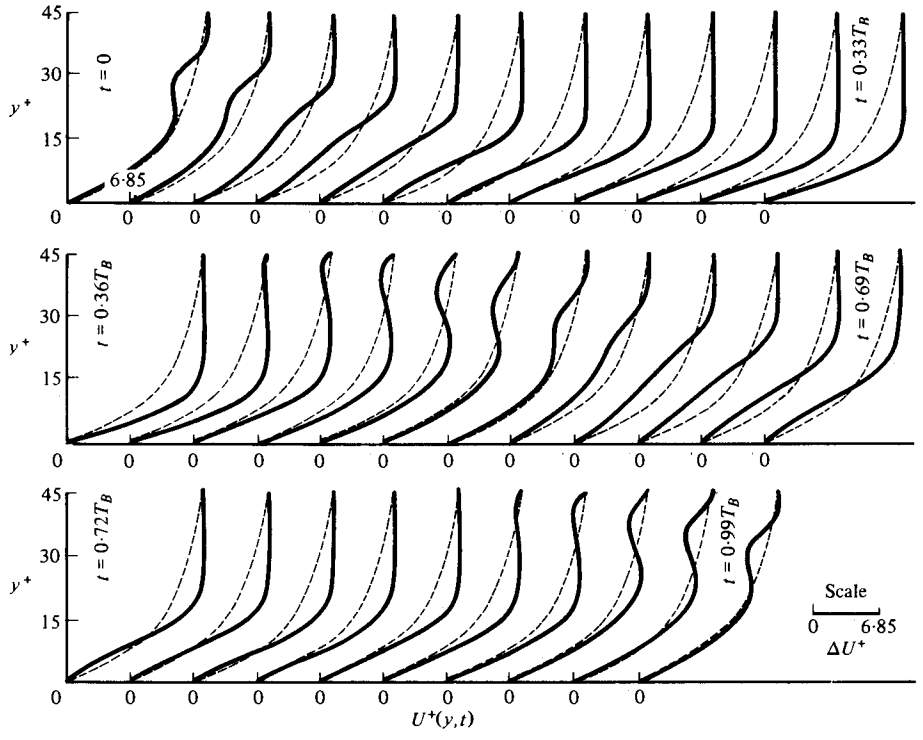

FIGURE 6. Calculated instantaneous axial velocity profiles, $y_0^+ = 45$, $\lambda^+ = 100$ and $T_B^+ = 100$, at $Z^+ = 22$ and for times $t = 0$ to $t = 0{\cdot}99T_B$.

to the wall region. During the acceleration, inflexion points gradually disappear from the axial velocity profile and a blunt velocity profile with a region of uniform velocity expanding from the upper boundary toward the wall develops.

At $t \cong 0{\cdot}35T_B$ a deceleration of the axial velocity profile begins and continues to $t \cong 0{\cdot}79T_B$. This deceleration occurs over the period that outflows are occurring at $z = 0$. At $t = 0{\cdot}63T_B$ the axial velocity profile is the same as the mean profile. At subsequent times ($t = 0{\cdot}65T_B$ to $0{\cdot}84T_B$) a distinct shear layer is present at the upper boundary which separates the regions of coherent flow from the outer flow, as evidenced by a strong discontinuity in the axial velocity profile right at the upper boundary. This shear layer appears because of the movement of low momentum fluid from the wall. The discontinuity is a consequence of the assumption of a well mixed outer region. The change in the axial velocity might not be so sudden if a more sophisticated matching between the inner and outer flows were used. Negative deviations of the instantaneous axial velocity from the mean velocity profile are observed at all values of y for $t = 0{\cdot}84T_B$ to $t = 0{\cdot}91T_B$. However no shear layer is present at the upper boundary.

Figure 6 for $z = 0{\cdot}22\lambda$ shows that the velocity profiles alternate between acceleration and deceleration stages. The acceleration or deceleration always starts in the region close to the upper boundary. Viscous effects close to the wall slow down the rate of change of axial velocity. During the acceleration stages, inflexional points disappear from the velocity profiles, and blunt velocity profiles with regions of uniform

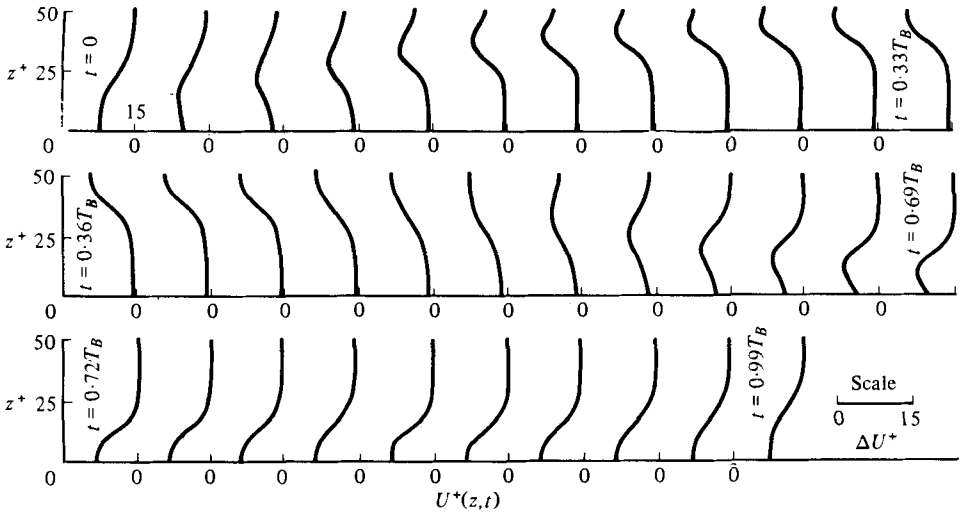

FIGURE 7. Calculated instantaneous axial velocities, $y_0^+ = 45$, $\lambda^+ = 100$ and $T_B^+ = 100$, at $y^+ = 18{\cdot}28$ and for times $t = 0$ to $t = 0{\cdot}99T_B$.

velocity, expanding from the upper boundary to the wall, appear. This is similar to what is observed in the axial velocity profiles at $z = 0$. However, instantaneous axial velocity profiles at $z = 0{\cdot}22\lambda$ never show steep discontinuities (shear layers) at the upper boundary as do the instantaneous profiles at $z = 0$.

There seems to be some differences in the literature in the definition of the actual event of bursting. We have chosen to define bursting as that period over which there is strong efflux of negative momentum to the outer flow. It is evidenced in these calculations by discontinuities at the upper boundary, $t = 0{\cdot}65T_B$ to $t = 0{\cdot}84T_B$. (At $z = 0{\cdot}50\lambda$, it occurs from $t = 0{\cdot}15T_B$ to $t = 0{\cdot}34T_B$.) It is to be noted that according to the above definition, dye streamers formed at a wall slot would disappear from the $z = 0$ location shortly after the bursting. The above definition of bursting implies that it occurs about 20 per cent of the time and that it occupies a region of thickness $\Delta z^+ < 44$. This result is in agreement with an estimate of 18 per cent by Corino & Brodkey (1969). The calculated profiles shown in figure 5 are in striking agreement with measured velocities for $y < 0{\cdot}4$ in. presented by Kim *et al.* (1971) in figure 6 of their paper. The following paraphrased description of the change of the velocity profile over a bursting cycle is given by them: Initially, the profiles show positive deviations from the mean velocity profile. In subsequent times the instantaneous axial velocity decreases until the profile resembles closely that of the mean profile. Further deceleration results in the formation of discontinuities of the axial velocity. The next stage is an acceleration of the fluid which starts at the upper boundary and moves toward the wall.

The properties of the calculated velocity profiles seem consistent with a number of other experimental results reported in the literature. During the deceleration phase deficiencies as high as 50 percent are observed in the instantaneous velocity profile in agreement with observations made by Nychas, Hershey & Brodkey (1973). Grass (1971) has observed that inrushes of fluid to the wall are associated with acceleration and ejections of fluid from the wall with deceleration of the axial velocity.

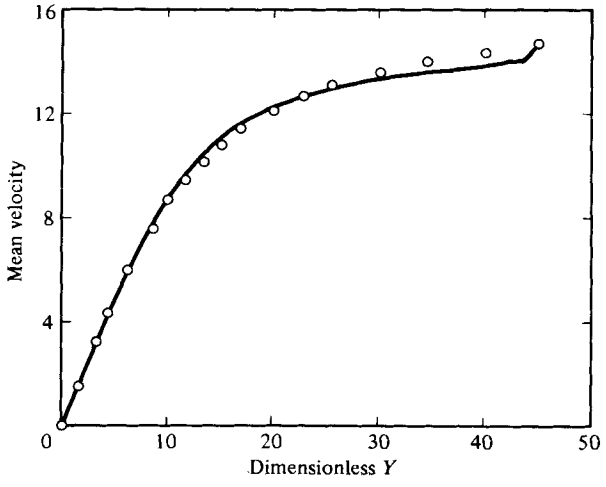

FIGURE 8. Comparison of a calculated mean velocity profile, $y_0^+ = 45$, $\lambda^+ = 100$ and $T_B^+ = 100$, with measurements by Laufer (1954).

In figure 7 calculated axial velocity profiles at $y^+ = 18{\cdot}28$ are shown. A common feature of all of these profiles is the large spanwise variation of the axial velocity. The ratio of the axial velocities between the faster and slower moving fluid varies between 1·5 and 2·5. Kline *et al.* (1967) from their measurements, found that this ratio varies between 1·2 and 2·9. From figure 6 it is seen that a region of low speed fluid, which is the result of the movement of momentum deficient fluid outward from the boundary, appears alternately at the two boundaries, $z = 0$ and $z = \frac{1}{2}\lambda$ as the region of maximum outflow shifts between 0 and $\frac{1}{2}\lambda$.

It can also be seen that the spanwise extent of the high speed region is larger than the spanwise extent of the low speed region. At certain times large changes in axial velocity are noted to occur over a small region. This coexistence of fluids of quite different velocity has been observed experimentally by Corino & Brodkey (1969) and described by them as a two-layer velocity field. Hinze (1975) has described it as a 'vertical' shear layer and has pointed out that it may be a region of high viscous dissipation. In agreement with the calculations presented in figure 6 Schraub & Kline (1965) observed that at $y^+ \cong 10$ the high speed streaks are wider than the low-speed streaks and Kim *et al.* (1971) determined that the spanwise extent of a low speed streak is $z^+ \cong 10$–30.

6. Statistical analysis

In the previous three sections calculated properties of the instantaneous velocity field were compared with observations. In this section average properties are compared to measured statistical properties of wall turbulence. Averages at a given y^+ were obtained by averaging over one period in time and half the wavelength in z. Two sets of parameters were used in these calculations $y_0^+ = 38$, $\lambda^+ = 100$, $T_B^+ = 90$ and $y_0^+ = 45$, $\lambda^+ = 100$, $T_B^+ = 100$.

Figure 8 compares the calculated average velocity profile with that measured by Laufer (1954). Here the average velocity has been normalized with the friction velocity.

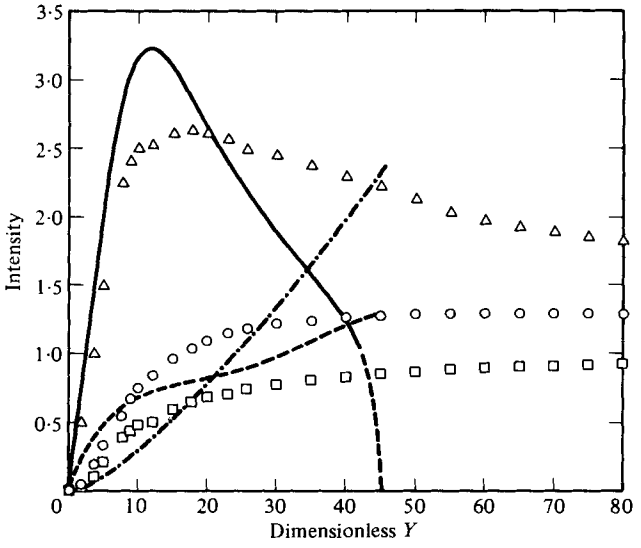

FIGURE 9. Comparisons of calculated turbulent intensities, $y_0^+ = 45$, $\lambda^+ = 100$ and $T_B^+ = 100$, with measurements by Laufer (1954). △, u^+; □, v^+; ○, w^+.

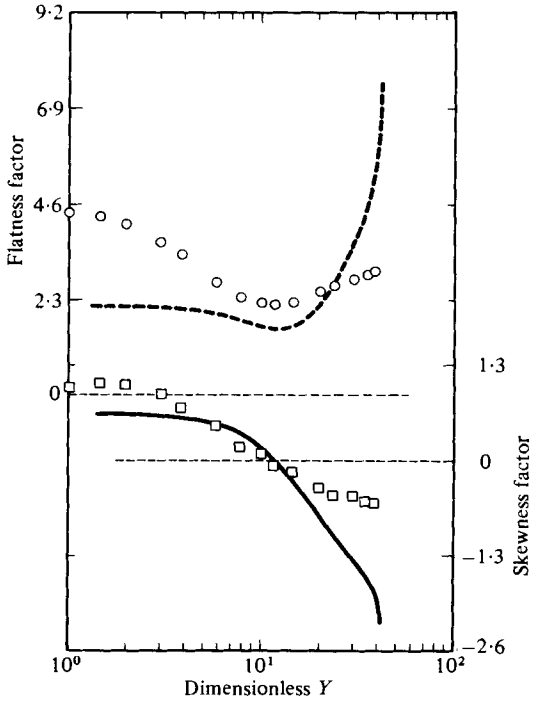

FIGURE 10 Comparison of calculated skewness and flatness, $y_0^+ = 38$, $\lambda^+ = 100$ and $T_B^+ = 90$, with measurements by Kreplin (Eckelmann 1974).

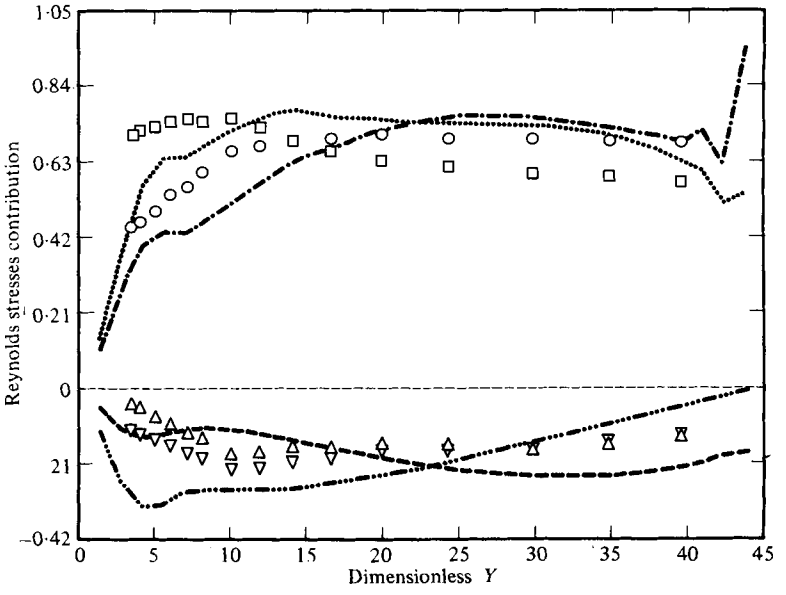

FIGURE 11. Comparison of calculated classified Reynolds stresses, $y_0^+ = 45$, $\lambda^+ = 100$ and $T_B^+ = 100$, with measurements by Brodkey *et al.* (1974). ▽−−−▽, quadrant I; ○−·−·−○, quadrant II; △−···−△, quadrant III; □.....□, quadrant IV.

Good agreement is noted particularly for $y^+ < 25$. The region $y^+ > 25$ appears to provide a reasonable match for the relation

$$\bar{U}^+ = 5{\cdot}60 \log y^+ + 5{\cdot}0. \tag{19}$$

Calculated dimensionless intensities are compared with Laufer's (1954) measurements in figure 9. A number of features of the calculated intensities are in good agreement with measurements. A maximum in $\overline{u^2}$ is calculated at $y^+ \cong 10$, close to the value at which measured values of $\overline{u^2}$ show a maximum. From the slopes of the $(\overline{u^2})^{\frac{1}{2}}$ and $(\overline{w^2})^{\frac{1}{2}}$ curves at $y = 0$, values of $(\overline{s_x^2})^{\frac{1}{2}}$ and $(\overline{s_z^2})^{\frac{1}{2}}$ can be calculated. It is noted that this ratio is approximately equal to three, in agreement with measurements. The calculated axial velocity fluctuations at large y^+ are too small. This is a consequence of the simple matching that is used, in particular, the assumption of a constant axial velocity, U_L, in the well mixed region. The calculated normal velocity fluctuations are too large at large y^+, reflecting the fact that the assumption of a completely coherent motion up to y_0^+ is only an approximation.

Figure 10 compares values of the skewness and the flatness of the turbulent axial velocity with the measurements of Kreplin (Eckelmann 1974). The calculated skewness is positive for $y^+ < 12$ and negative for $y^+ > 12$. The calculated flatness has a minimum at $y^+ \cong 12$. The above features have also been observed in experiments by Eckelmann (1974), Zaric (1972), Ueda & Hinze (1975) and Ueda & Mitzushina (1977).

As in Willmarth & Lu (1971) and Wallace, Eckelmann & Brodkey (1972), calculated time averaged values of the product uv have been classified according to the sign of its components u and v in figure 10. Quadrant IV ($u > 0$, $v < 0$) is identified as inflows of high-speed fluid, quadrant II ($u < 0$, $v > 0$), as ejections of low-speed fluid and

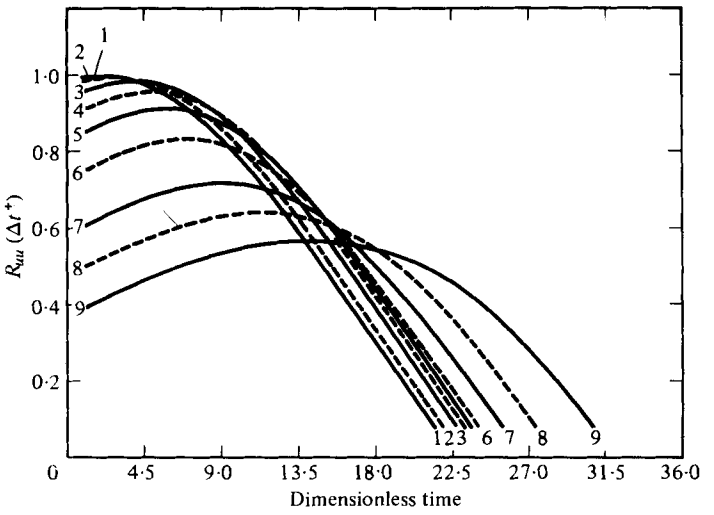

FIGURE 12. Calculated space–time correlation of u, $y_0^+ = 38$, $\lambda^+ = 100$, $T_B^+ = 90$. $\Delta x^+ = 0$, $\Delta z^+ = 0$ $y_{ref} = 1{\cdot}9$. 1, $\Delta y^+ = 3{\cdot}563$; 2, $\Delta y^+ = 4{\cdot}750$; 3, $\Delta y^+ = 7{\cdot}125$; 4, $\Delta y^+ = 9{\cdot}500$; 5, $\Delta y^+ = 11{\cdot}875$; 6, $\Delta y^+ = 15{\cdot}438$; 7, $\Delta y^+ = 21{\cdot}375$; 8, $\Delta y^+ = 27{\cdot}313$; 9, $\Delta y^+ = 33{\cdot}250$.

quadrants I ($u > 0$, $v > 0$) and II ($u < 0$, $v < 0$) as interactions between inflows and outflows. As seen in figure 11 the calculations agree with experiments (Brodkey *et al.* 1974) in that quadrants IV and II each contribute approximately 70 per cent to the Reynolds stress and quadrants I and II contribute -40 per cent. Also in agreement with experiments the quadrant IV contribution is greater than the quadrant II contribution for $y^+ < 22$.

All of the calculations of statistical quantities shown in figures 8, 9, 10 and 11 were done for $y_0^+ = 45$, $\lambda^+ = 100$, $T_B^+ = 100$. Results for $y_0^+ = 38$, $\lambda^+ = 100$, $T_B^+ = 90$ were the same except for some minor differences: They showed a smoother variation of $(\overline{w^2})^{\frac{1}{2}}$ with y^+, a change in the sign of the skewness at $y^+ = 10$, and a change in the relative importance of the contribution of quadrant IV and of quadrant II to the Reynolds stress at $y^+ = 18$.

Space time correlations of the axial velocity were calculated only for $y_0^+ = 38$, $\lambda^+ = 100$, $T_B^+ = 90$. These are shown in figure 12. The separation is in a direction normal to the wall. In agreement with experiments (Eckelmann 1974; Ueda & Mitzushina 1977) the u pattern close to the wall lags behind the u pattern far from the wall. The time at which the space-time correlation reaches its maximum increases with separation distance Δy^+. From the same figure it is seen that the axial correlation with zero time delay, $R_{uu}(0, \Delta y)$ ($y_{ref} = 0$, $\Delta x = 0$, $\Delta z = 0$, $\Delta t = 0$), decreases with increasing separation distance y, indicating that coherency need not require a correlation of unity. This decrease in $R_{uu}(0, \Delta y)$ is a consequence of the change of the phases of the velocity fluctuations with distance from the wall that is reflected in the time variation of the structure.

7. Selection of parameters

The parameters used in this model are either associated with the dimensions of the region of coherent motions (y_0, λ) or with the boundary conditions for the velocity at the upper boundary (T_B, λ, w_L, U_L). In § 3 it was mentioned that w_L and U_L are determined from the conditions

$$\left.\begin{aligned} \frac{(\overline{w^2})^{\frac{1}{2}}}{u^*} &= 1{\cdot}30 \\ \frac{d(\overline{w^2})^{\frac{1}{2}}}{dy} &= 0 \end{aligned}\right\} \quad \text{for} \quad y^+ > 30 \tag{20}$$

and

$$U_L \simeq \overline{U}(y_0), \tag{21}$$

respectively. These restrictions reduced the number of parameters at our disposal to three.

The spanwise length of the region of coherent motions, λ, is taken to be equal to the spanwise spacing of the dye streaks which, for turbulent flows over a smooth and plane wall, has been determined experimentally to be $\lambda^+ = 100 \pm 20$ (Kline *et al.* 1967; Kim *et al.* 1971).

The selection of the upper boundary was largely based on the visual observations of Kline *et al.* (1967). They observed that fluid in low speed regions moves slowly downstream in the region $0 < y^+ < 10$. At the initiation of a burst this fluid was observed to move quickly away from the wall in the region $10 < y^+ < 40$ and to break up into chaotic motions in the region $y^+ > 40$. This description also seems to be in accord with visual observations by Corino & Brodkey (1969) and Nychas *et al.* (1973). However, there seems to be some variation in the definition of the region where chaotic motion is initiated. From these considerations we have used $y_0^+ = 40 \pm 10$.

A period for the spanwise disturbances that is consistent with the observed bursting period was selected. However, since it is tacitly assumed that these disturbances contain most of the turbulent energy in the viscous sublayer, it seems desirable that their frequency correspond to the median frequency of the spectrum of the velocity fluctuations close to the wall. Hanratty *et al.* (1977) summarize measurements of the spectrum of the fluctuations of the wall velocity gradient, in pipe flows made in our laboratory and of the x component of the turbulent velocity fluctuations made in pipe flows by Bakewell & Lumley (1967) at $y^+ = 2{\cdot}56$ and by Laufer (1954) at $y^+ = 5{\cdot}91$. Over the range of Reynolds numbers covered in these experiments it is found that the median frequency in Hertz is $f_m = 0{\cdot}9 \times 10^{-2}\, u^{*2}/\nu$. The visual measurements of the bursting frequency by Schraub & Kline and by Runstadler, Kline & Reynolds (summarized by Kim *et al.* 1971) give a bursting frequency of $f_B \cong 10^{-2}\, u^{*2}/\nu$ in close agreement with the median frequency of the velocity fluctuations. Estimates of the bursting period made by analysing velocity signals from a hot wire anemometer are summarized by Laufer & Narayanan (1971). These indicate that $f_B \nu/u^{*2}$ decreases with increasing Reynolds number. However, as pointed out by Kim *et al.* (1971), there is a need to check these hot wire techniques directly against visual observations to insure that the two are directly related. On the basis of the above considerations we have chosen T_B^+ as apprxomately equal to λ^+. If the suggestion of Laufer &

Narayanan is correct the bursting period is much larger than the period of the energy containing eddies at very large Reynolds numbers and the model presented in this paper would not represent flow fluctuations at very large Reynolds numbers.

The model intends to describe the kinematics of a coherent flow which has strong convective motions. This requirement can be met if in the equations of motion the inertia and transient terms are equally important. The ratio of these terms is

$$\frac{\text{inertia terms}}{\text{transient terms}} \sim \frac{w_L^+ T_B^+}{\lambda^+}. \tag{22}$$

Since w_L^+ is of order unity, the above choice of T_B^+ and λ^+ would satisfy this condition. A similar order of magnitude analysis gives

$$\frac{\text{viscous terms}}{\text{transient terms}} \sim \frac{T_B^+}{\delta_v^{+2}} \tag{23}$$

and

$$\frac{\text{viscous terms}}{\text{inertia terms}} \sim \frac{\lambda^+}{w_L^+ \delta_v^{+2}}, \tag{24}$$

where δ_v^+ is the dimensionless distance from the wall over which viscous effects are important. From the above, the following estimate of δ_v^+ is obtained:

$$\min\left[\left(\frac{T_B^+}{\lambda^{+2}}\right)^{\frac{1}{2}}, \left(\frac{1}{w_L^+ \lambda^+}\right)^{\frac{1}{2}}\right] \leqslant \frac{\delta_v^+}{\lambda^+} \leqslant \max\left[\left(\frac{T_B^+}{\lambda^{+2}}\right)^{\frac{1}{2}}, \left(\frac{1}{w_L^+ \lambda^+}\right)^{\frac{1}{2}}\right]. \tag{25}$$

Thus for our choices of λ^+ and τ^+ the term $\delta_v^+/\lambda^+ = O(10^{-1})$ and δ_v^+ will be much smaller than y_0^+.

There is some leeway, within the above stated bounds, in the choice of λ^+, T_B^+, y_0^+. We explored a number of possibilities and settled on the following further criteria for final choices with which to examine the details of the calculated flow field: (1) The mean velocity profile in the immediate vicinity of the wall satisfies the relation $\overline{U}^+ = y^+$. (2) The calculated relation for the variation of the spanwise intensity is reasonably smooth throughout the viscous wall region. Our choice of the second criteria was associated with belief that this might be more consistent with the assumption of coherency. There are a number of triplets $(y_0^+, \lambda^+, T_B^+)$ which satisfy the above two criteria. Two of these ($y_0^+ = 45$, $\lambda^+ = 100$, $T_B^+ = 100$) and ($y_0^+ = 38$, $\lambda^+ = 100$, $T_B^+ = 90$) were discussed in the previous section.

Hatziavramidis (1978) has presented calculated profiles of the average velocity and of the turbulent intensities for a number of different cases. However, the influence of T_B^+ and λ^+ could not be defined because of the expense that would be involved in doing a sufficiently comprehensive study to come to any definite conclusions. We will just cite some of his results here.

Calculations for $y_0^+ = 38$, $T_B^+ = 90$ and $\lambda^+ = 50, 100, 150$ showed that the influence of increasing λ^+ was to decrease the slope of the $\overline{U}^+$ *versus* y^+ relation at $y^+ \to 0$; i.e. to cause drag-reduction. The profile of $(\overline{w^2})^{\frac{1}{2}}$ for $\lambda^+ = 150$ showed almost a monotonic decrease of the slope, whereas decreasing the value of λ^+ made this profile more inflexional.

Calculations for $y_0 = 45$, $\lambda^+ = 100$, $T_B^+ = 40$ gave a slope of the mean velocity at $y^+ \to 0$ significantly greater than unity, i.e. a drag increase. The profile of the transverse

turbulent velocity profile for this case showed a minimum between $y^+ = 20$ and $y^+ = 30$.

Calculations for $T_B^+ = 100$, $\lambda^+ = 100$ and $y_0^+ = 32, 38, 45$ showed that the slope of mean velocity profile at $y^+ \to 0$ decreased with increasing y_0^+. The profile of the transverse turbulent velocity for $y_0^+ = 32$ showed a smoothly decreasing slope. The profile of the transverse velocity for the other two cases was inflexional but did not show any minimum.

8. Closure

The rather good agreement between the calculations presented in this paper and qualitative aspects of presently available measurements suggests that many of the observed phenomena in the viscous wall layer are a consequence of a viscous interaction between the turbulent flow and the wall caused by slight spanwise deviations from the mean flow direction of the fluid at $y^+ \cong 30$. The calculations suggest that if the lateral scale and the period of these deviations are approximately equal to the spacing of the observed streaky structure and the time interval between bursts, a localized rather large outward flow of low momentum fluid from the viscous wall region to the outer flow occurs periodically. We identify these events as 'bursts'.

The paper does not attempt to examine the influence this flow of low momentum fluid from the wall on the generation of turbulence in the outer flow or on the determination of λ^+ or T_B^+. Consequently, as pointed out in the introduction, it does not answer the question of whether the viscous wall region is 'passive' or drives the turbulence throughout the boundary layer.

In addition to the obvious limitation of representing turbulence with a regular eddy pattern there are a number of other shortcomings of this model. These include the rather simple method of matching a completely coherent inner flow with well-mixed outer flow, the specification of the conditions in the outer flow and the assumption of homogeneity in the x direction.

The comparison of calculated results with measurements indicates that the flow is not completely coherent up to $y^+ = 30$. The values of the spatial correlation shown in figure 12 are larger than the measurements reported by Eckelmann (1974). In addition, the assumption of complete coherency up to $y^+ = 30$ requires much larger values of the normal velocity at the edge of the viscous wall layer than is indicated by measurements. These comparisons indicate that the assumption of coherency is reasonably accurate for $y^+ < 15$ but becomes less acceptable for $y^+ > 15$.

The use of $u = U_L = \text{constant}$ as a boundary condition at the edge of the viscous wall layer is responsible for the sharp drop in the calculated values of $\overline{u^2}$ for large y^+. As illustrated by Fortuna in the development of his pseudo-steady state model (1970), the allowance of U_L to be a function of time gives a calculated $\overline{u^2}$ variation with y^+ which is in much better accord with measurements. It is of interest to note that even though $\overline{u^2}$ is assumed to be zero in the well mixed region, large values of $\overline{u^2}$ are generated in the viscous wall region by the secondary flow. Fortuna (1970) has suggested that the oscillations in u at $y = y_0$ are simply dampened in the viscous wall layer so that the experimentally observed maximum in $\overline{u^2}$ is probably the result of the contributions to x velocity fluctuations from the secondary flow.

In addition to making large contributions to the velocity fluctuations close to a wall, the secondary flow also appears to be a major factor in determining the Reynold stress. This is evidenced by the good agreement with experiments of the calculations of the mean velocity profile and of the quadrant analysis of the Reynolds stress (see figure 11).

Even though measurements of spatial correlation coefficients support the assumption of homogeneity in the x direction, there are a number of visual observations of localized disturbances for which the model cannot account. Since these events could be the result of an instability, it is not clear that the simple inclusion of convective terms in the x direction in the model equations would predict such events. Therefore, it did not seem advantageous to us to forgo the simplifications involved in decoupling the x momentum equation from the y and z momentum equations in order to explore the influence of non-homogeneities in the mean flow direction.

This work is supported by the Office of Naval Research under Grant NR 062-558.

REFERENCES

Aziz, K. & Hellums, J. C. 1967 *Phys. Fluids* **10**, 314.

Bakewell, H. P. & Lumley, J. L. 1967 *Phys. Fluids* **10**, 1800.

Blackwelder, R. F. & Kaplan, R. E. 1972 *12th Symp. IUTAM.*

Brodkey, R. S., Wallace, J. M. & Eckelmann, H. 1974 *J. Fluid Mech.* **63**, 209.

Corino, E. R. & Brodkey, R. S. 1969 *J. Fluid Mech.* **37**, 1.

Corrsin, S. 1956 *Symp. on Naval Hydrodyn.*

Eckelman, L. D. 1971 The Structure of Wall Turbulence and its Relation to Eddy Transport. Ph.D. thesis, Department of Chemical Engineering, University of Illinois, Urbana.

Eckelmann, H. 1974 *J. Fluid Mech.* **65**, 439.

Fage, F. A. & Townsend, H. C. H. 1932 *Proc. Roy. Soc.* A **135**, 656.

Fortuna, G. 1970 Effect of Drag Reducing Polymers on Flow Near a Wall. Ph.D. thesis, Department of Chemical Engineering, University of Illinois, Urbana.

Fortuna, G., Gilead & Hanratty, T. J. 1972 *J. Fluid Mech.* **53**, 575.

Frankel, S. P. 1950 *Math Tables and Other Aids to Computation* **4**, 65.

Grass, A. J. 1971 *J. Fluid Mech.* **50**, 233.

Gurkham, A. A. & Kader, B. A. 1970 *Paris Heat Transfer Conf.*, FC 2, p. 5.

Hanratty, T. J., Chorn, L. G. & Hatziavramidis, D. T. 1977 *Phys. Fluids Suppl.*

Hatziavramidis, D. T. 1978 Interpretation of the Flow in the Viscous Wall Region as a Driven Flow. Ph.D. thesis, Department of Chemical Engineering, University of Illinois, Urbana.

Hinze, J. O. 1975 *Turbulence*, 2nd ed.

Kim, H. T., Kline, S. J. & Reynolds, W. C. 1971 *J. Fluid Mech.* **50**, 133.

Kline, S. J. & Runstadler, P. W. 1959 *J. Appl. Mech.* **2**, 166.

Kline, S. J., Reynolds, W. C., Schraub, F. A. & Runstadler, P. W. 1967 *J. Fluid Mech.* **30**, 741.

Landahl, M. T. 1972 *J. Fluid Mech.* **56**, 775.

Laufer, J. 1954 *N.A.C.A. Rep.* 1174.

Laufer, J. & Narayanan, M. A. B. 1971 *Phys. Fluids* **14**, 182.

Lee, M. K., Eckelman, L. D. & Hanratty, T. J. 1974 *J. Fluid Mech.* **66**, 17.

Mitchell, J. E. & Hanratty, T. J. 1966 *J. Fluid Mech.* **26**, 199.

Mollo-Christensen, E. 1971 *A.I.A.A. J.* **9**, 1217.

Nychas, S. G., Hershey, H. C. & Brodkey, R. S. 1973 *J. Fluid Mech.* **61**, 513.

OFFEN, G. R. & KLINE, S. J. 1975 *J. Fluid Mech.* **70**, 209.

PEACEMAN, D. W. & RACHFORD, H. H. 1955 *J. Soc. Ind. Appl. Math.* **3**, 28.

PEARSON, C. A. 1965 *J. Fluid Mech.* **21**, 611.

SCHRAUB, F. A. & KLINE, S. J. 1965 *Thermosci. Div., Mech. Eng. Dept.* Rep. No. MD-12. Stanford University.

SCHUBERT, G. & CORCOS, G. M. 1967 *J. Fluid Mech.* **29**, 113.

STERNBERG, J. 1962 *J. Fluid Mech.* **13**, 241.

STERNBERG, J. 1965 *AGARD* 97.

TAYLOR, G. I. 1932 *Proc. Roy. Soc.* A **135**, 678.

TOWNSEND, A. A. 1956 *The Structure of Turbulent Shear Flow.*

UEDA, H. & HINZE, J. O. 1975 *J. Fluid Mech.* **67**, 125.

UEDA, H. & MITZUSHINA, T. 1977 *Proc. Symp. on Turbulence in Liquids* 41.

WALLACE, J. M., ECKELMANN, J. & BRODKEY, R. S. 1972 *J. Fluid Mech.* **54**, 39.

WILLMARTH, W. W. & LU, S. S. 1971 *J. Fluid Mech.* **55**, 481.

ZARIC, Z. 1972 *4th All Union Heat Mass Transfer Conf.*